Science of the Total Environment 677 (2019) 732–744

Contents lists available at ScienceDirect

Science of the Total Environment

journal homepage: www.elsevier.com/locate/scitotenv

Aggravating O_3 pollution due to NO_x emission control in eastern China

Nan Wang [a,b,d], Xiaopu Lyu [c], Xuejiao Deng [d], Xin Huang [a,b,*], Fei Jiang [e], Aijun Ding [a,b]

[a] Joint International Research Laboratory of Atmospheric and Earth System Sciences, School of Atmospheric Sciences, Nanjing University, Nanjing, China
[b] Jiangsu Provincial Collaborative Innovation Center for Climate Change, Nanjing, China
[c] Department of Civil and Environmental Engineering, Hong Kong Polytechnic University, Hong Kong
[d] Institute of Tropical and Marine Meteorology, China Meteorological Administration, Guangzhou, China
[e] Jiangsu Provincial Key Laboratory of Geographic Information Science and Technology, International Institute for Earth System Science, Nanjing University, Nanjing 210023, China

HIGHLIGHTS

- China witnessed a drop of NOx and growing O_3 pollution in recent years.
- O_3 formation in East China has gradually changed to mixed sensitive regime
- VOCs-targeted emission control is a feasible way for China's O_3 mitigation.

GRAPHICAL ABSTRACT

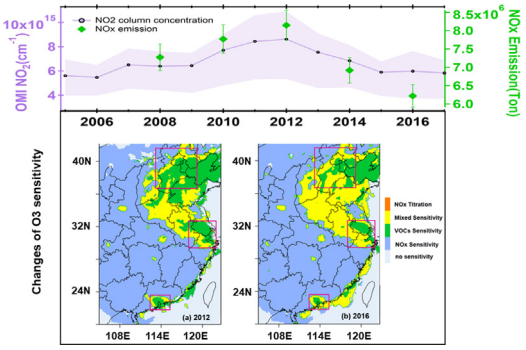

ARTICLE INFO

Article history:
Received 9 March 2019
Received in revised form 25 April 2019
Accepted 26 April 2019
Available online 28 April 2019

Editor: Jianmin Chen

Keywords:
Ozone pollution
Emission sensitivity
WRF-CMAQ
Policy application

ABSTRACT

During the past five years, China has witnessed a rapid drop of nitrogen oxides (NO_x) owing to the wildly-applied rigorous emission control strategies across the country. However, ozone (O_3) pollution was found to steadily deteriorate in most part of eastern China, especially in developed regions such as Jing-Jin-Ji (JJJ), Yangtze River Delta region (YRD) and Pearl River Delta region (PRD). To shed more light on current O_3 pollution and its responses to precursor emissions, we integrate satellite retrievals, ground-based measurements together with regional numerical simulation in this study. It is indicated by multiple sets of observational data that NO_x in eastern China has declined more than 25% from 2012 to 2016. Based on chemical transport modeling, we find that O_3 formation in eastern China has changed from volatile organic compounds (VOCs) sensitive regime to the mixed sensitive regime due to NO_x reductions, substantially contributing to the recent increasing trend in urban O_3. In addition, such transitions tend to bring about an ~1–1.5 h earlier peak of net O_3 formation rate. We further studied the O_3 precursors relationships by conducting tens of sensitivity simulations to explore potential ways for effective O_3 mitigation. It is suggested that the past control measures that only focused on NO_x may not work or even aggravate O_3 pollution in the city clusters. In practice, O_3 pollution in the three regions is expected to be effectively mitigated only when the reduction ratio of VOCs/NO_x is greater than 2:1, indicating VOCs-targeted control is a more practical and feasible way.

* Corresponding author at: Joint International Research Laboratory of Atmospheric and Earth System Sciences, School of Atmospheric Sciences, Nanjing University, Nanjing, China.
E-mail address: xinhuang@nju.edu.cn (X. Huang).

https://doi.org/10.1016/j.scitotenv.2019.04.388
0048-9697/

1. Introduction

Characterized by high levels of particulate matters ($PM_{2.5}$), high mixing ratio of ozone (O_3) and low visibility, air pollution in China has attracted lots of attention worldwide. In fact, China has been dedicating to fighting against air pollution in the past decades. Due to the continuous efforts on emission control and restriction, the increase of $PM_{2.5}$ has been somewhat alleviated and even reversed (He et al., 2017; Song et al., 2017). However, photochemical O_3 pollution is still serious (annual increasing rate is 6.5 μg/m^3 from 2013 to 2017, data source: the Ministry of Ecology and Environment of China, http://www.mee.gov.cn/, last access on 25 April 2019) and frequently deteriorate atmospheric environment especially in eastern China, where the highly developed city clusters such as the Beijing-Tianjin-Hebei (JJJ) area, Yangtze River Delta (YRD) region and Pearl River Delta (PRD) region are located.

Tropospheric O_3 is produced by emissions of nitrogen oxides ($NO_x = NO + NO_2$) and volatile organic compounds (VOCs) in the presence of sunlight (Atkinson, 2000). It is not only harmful to human health but also poses adverse impact on plants and even ecosystem (Booker et al., 2009; Fann et al., 2012; Brauer et al., 2016; Lin et al., 2018). As one of the greenhouse gases, O_3 also affects global climate (Watson et al., 1990; Shindell, 2004; de_Richter and Caillol, 2011). The control of O_3 is of great challenge due to the complicated and non-linear relationship between O_3 and its precursors (Xing et al., 2011; Ou et al., 2016). Briefly, net O_3 is produced when the photo-stationary state between O_3 and NO_x, i.e., $NO_2 + O_2 + M \leftrightharpoons NO + O_3 + M$, are destroyed by the intervention of alkylperoxyl (RO_2) and hydroperoxyl (HO_2) from VOCs and CO, which lead to the oxidization of NO to NO_2 ($RO_2 + NO + O_2 -> HO_2 + NO_2$; $HO_2 + NO -> OH + NO_2$), resulting in net O_3 accumulation via NO_2 photolysis finally (Atkinson, 2000). The relationship between O_3 and its precursors is usually identified as VOCs-sensitive, NO_x-sensitive or mix-sensitive. In general, a VOCs-sensitive regime means that reducing VOCs emissions could lead to the reduction of RO_2, which accordingly decreases the transition of NO to NO_2 and finally results in lower O_3 production; In NO_x-sensitive regimes, NO serves as the limiting regent in reactions with RO_2 and HO_2. Thus, O_3 production can be restricted by cutting NO_x emissions. The mix-sensitive regime, however, enables the reduction of O_3 by lowering the emissions of either VOCs, NO_x, or both (Sillman, 2002; Sillman, 2003; Sillman and West, 2009; Xie et al., 2014; Xue et al., 2014; Jin and Holloway, 2015).

Current methods to identify the O_3-NO_x-VOCs sensitivity include the observation-based methods, satellite retrievals and model approaches. Usually, the field observations can directly provide information of O_3 and its precursors and it is feasible to calculate O_3 sensitivity by applying the observe-based models. For example, Ling et al. (2013) investigated O_3 sensitivity in Hong Kong with a photochemical box model constrained by observed VOCs and NO_x data. The method can provide accurate in-situ diagnoses of O_3 sensitivity but is limited in temporal and spatial extent (Wang et al., 2017). Satellite retrievals, based on the ratio of formaldehyde (HCHO) to NO_2, are also widely used. It overcomes the limit of field measurements and provides data in time and space. Martin et al. (2004) adopted the retrievals from GOME (Global Ozone Monitoring Experient) and investigated O_3 sensitivity of Northern Hemisphere. However, these kinds of top-down observations are affected by clouds, aerosols, precipitations and ground reflectivity, hence certain inherent uncertainties (De Smedt et al., 2010). Besides, most satellites provide only once-a-day observations, which could not reflect the diurnal variation. Modeling approaches, based on emission inventories of air pollutants, provide adequate descriptions of chemical species and chemical sensitivities to precursors across time (from hourly to yearly) and space (from ~1 km to ~100 km). Though air quality model also involves uncertainties mainly from emission inventories, it is a powerful regulatory tool in simulating the air quality and developing the science-based policies. (Xing et al., 2011; Li et al., 2013a, 2013b; Wang et al., 2016; Sun et al., 2019).

In eastern China, there has been many studies conducted to explore O_3-NO_x-VOCs sensitivity before the recent 5 years. Due to the large amount of NO_x emissions from diverse sectors, like transportation, industries residence and power plants, it has been acknowledged that the urban O3 formations are generally VOCs sensitive (Shao et al., 2009a, 2009b; Wang et al., 2009; Chou et al., 2009; Sun et al., 2011; Xing et al., 2011). For example, Wang et al. (2010) used the ratio of O_3 and NO_z (the sum of all reactive nitrogen oxides excluding NO_x) as an indicator to define the O_3-NO_x-VOCs sensitivity and reported that Beijing (capital, the most developed city in JJJ) was under a strong VOCs-sensitive regime in O_3 formation. Ding et al. (2013a) suggested that Nanjing, a developed city in YRD, was located in VOCs sensitive regimes according to observations of NO_y (collective name for oxidized forms of nitrogen in the atmosphere), O_3 and CO. Consistently, Shao et al. (2009a, 2009b) found that urban areas of Guangzhou in PRD was also sensitive to VOCs through an observation-based model. In contrast, studies concluded that the NO_x sensitive or mixed sensitive regimes dominated O_3 formation in the rural areas of eastern China (Wang et al., 2009; Xing et al., 2011; Jin et al., 2017).

Most of the above-mentioned studies were based on in-situ study or on a small region using earlier data. These hamper the application of the results to the current situations across China, especially after the implementation of the 12th *Five Year Plan* (FYP, 2010–2015) and *Atmospheric Prevention and Protection Action Plan* (APPAP, 2012–2017) when concerted efforts have been made to control the emission of NO_x (and also SO_2). Discernable improvement of air quality has been reported, with the decrease of $PM_{2.5}$ (He et al., 2017; Song et al., 2017). Very recently, Li et al. (2019) indicated that the notable drop of $PM_{2.5}$ was a main factor leading to the O_3 increment in the North China Plain, due to the release of HO_2 from its uptake on $PM_{2.5}$. However, the changes of the O_3-NO_x-VOCs sensitivity driven by the reduction of NO_x emissions remain unclear. With the rising trend of O_3 year by year, governments and policymakers are keen to know the up-to-date O_3 sensitivities, particularly in the city clusters with intensive public concerns. In this study, we firstly went over the past NO_x abatement policies/strategies in China. Observations, including both satellite retrievals and ground-based air quality monitoring data were combined with emission inventories to figure out the effects of these actions on NO_x control. Further, multiple numerical simulations with a chemical transport model (CTM) was used to investigate the difference of O_3-NO_x-VOCs sensitivity between 2012 (when NO_x emissions reached the peak) and 2016 (when NO_x emissions noticeably reduced). The characteristics and variations of O_3-NO_x-VOCs sensitivity were compared and discussed. Finally, we probed deeply into understanding O_3-NO_x-VOCs regime in 2016 with the aim to provide scientific support for future O_3 abatement in China.

2. Method and material

2.1. Observational data and emission inventories

We used the operational Ozone Monitoring Instrument (OMI) NO_2 product to identify tropospheric NO_2 variations in eastern China. OMI incorporates one visible region (349-504 nm) and two UV region (264–311 nm and 307-383 nm) with a spectral resolution between 0.42 and 0.63 nm and a spatial resolution of 13 × 24 km^2 at nadir (Levelt et al., 2006; Jin et al., 2017). As a nadir-viewing spectrometer, OMI provides daily global coverage product with a local time around 13:30. In this study, we used tropospheric NO_2 products between 2005 and 2017 (DOMINO v2.0), which were developed by the Royal Netherlands Meteorological Institute. Generally, the DOMINO retrieval involves three steps. Firstly, using Differential Optical Absorption Spectroscopy (DOAS) technique to access NO_2 slant columns from OMI instrument; Secondly, separating the tropospheric and stratospheric contribution to the slant column; Finally, using the tropospheric air mass factor (AMF) to convert tropospheric slant column into a vertical

column (Boersma et al., 2004, 2007, 2011). To be noted that OMI data was affected by row anomalies since 2007, the DOMINO algorithm followed the Row Anomaly Flagging Rules and discarded the affected rows which introduce pollution. More details are given by Boersma et al. (2011).

Emissions of O_3 precursors, namely, NO_x and VOCs, were obtained from Multi-resolution Emission Inventory for China (MEIC, http://www.meicmodel.org/, last access: 28 Nov. 2018). Developed by Tsinghua University, MEIC has been openly accessible to public since 2010 and has been keeping updated for providing recent emission benchmark in China. It involves major atmospheric pollutants including SO_2, NO_x, CO, NMVOC, NH_3, $PM_{2.5}$, PM_{10}, BC and OC from sources like transportation, power plants, agriculture, residential and industry (He, 2012; Zhang et al., 2009; Zheng et al., 2018). MEIC provides emissions with a grid resolution of 0.25 × 0.25° and the data were linearly interpolated to the modeling grid (12 × 12 km) with consideration of the earth curvature effect. In this study, NO_x and VOCs emissions from 2008, 2010, 2012, 2014 and 2016 were analyzed aiming to understand variations of O_3 precursors in recent years. In addition, the 2012-based and 2016-based MEIC emission inventories were adopted to drive CTM modeling for the exploration of O_3 sensitivity in eastern China.

Ground-based monitoring data on ambient trace gases and meteorological field are collected for O_3 sensitivity analysis as well as model validation. Annual averages of NO_2 and O_3 concentrations were collected from China Statistical Yearbook by National Bureau of statics (2013–2017, available at http://www.stats.gov.cn/tjsj/ndsj/, in Chinese, last access: 28 Nov. 2018), which originated from Ministry of Environmental Protection (MEP) of China. Since 2013, national MEP had enlarged the operational air quality monitoring sites from 31 cities to 74 cities in China in order to provide more detailed monitoring information (GB3095-2012). Therefore, we showed yearly averages of NO_2 and O_3 from 74 cities between 2013 and 2017 in this study. Besides, hourly meteorological parameters (temperature, relative humidity (RH), wind) and trace gases (NO_x and O_3) were used to evaluate model performance (site distributions are illustrated in Fig. 1). Meteorological data and trace gases were obtained from operational surface monitoring stations maintained by China Meteorological Administration (CMA) and China Environmental Monitoring Center, respectively (CEMC). Our previous studies have demonstrated the good quality of these data (Ding et al., 2013a, 2013b; Wang et al., 2016; Xu et al., 2017; Huang et al., 2018).

2.2. Regional chemical transport model

A chemical transport model, i.e., Weather Research Forecast – Community Multiscale Air Quality (WRF-CMAQ) modeling system, was employed to investigate O_3 sensitivity in Eastern China. With the capability considering the complex interactions of atmospheric chemistry and physics, WRF-CMAQ modeling is widely used around the world ranging from atmospheric environment evaluation and policy analysis to understanding the complicated mechanism between air pollutants and meteorology (Gilliland et al., 2008; Wang et al., 2015; Wang et al., 2016). In this study, we applied two-nested domain with a grid resolution of 36 × 36 km and 12 × 12 km, respectively. The outer domain covered most area of China, parts of Southern China Sea and Western Pacific. The inner domain covered eastern China with JJJ, YRD and PRD being highly focused (Fig. 1). Vertically, there were 30 levels based on terrain-following hydrostatic-pressure coordinate, with the lowest level from the surface to the top of 100 hPa.

The WRF model (version 3.9.1) was performed to simulate weather conditions by using the 1° × 1° NCEP (National Centers for Environmental Prediction) FNL Operational Global Analysis data (https://rda.ucar.edu/datasets/ds083.2/, last access on April 25, 2019). Meanwhile, the NCEP ADP Global Upper Air Observational Weather Data (https://rda.ucar.edu/datasets/ds351.0/, last access on April 25, 2019) was assimilated to improve model performance on meteorology reproduction. The key configurations of WRF-CMAQ involved that, the Rapid

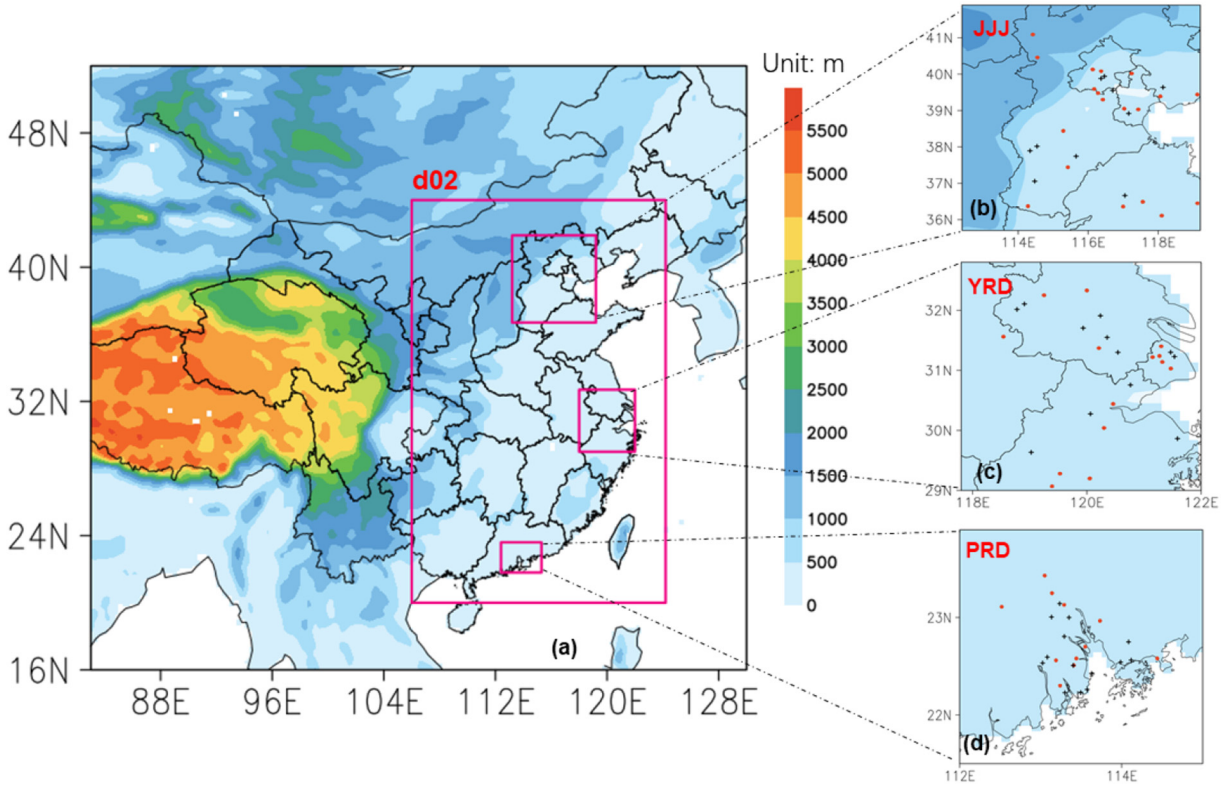

Fig. 1. Modeling domains and the 3 focused regions in eastern China (a), the contour is terrain height; and JJJ (b), YRD (c) and PRD (d). The red and black dots in b-d represents air quality monitoring stations (from CEMC) and weather monitoring stations (from CMA).

Radioactive Transfer Model (RRTM) for short and long wave radiation scheme, the Noah Land Surface Model for land-atmospheric interactions, the ACM2 boundary layer scheme, the Lin microphysics scheme, the Kain-Fritsch scheme for cumulus parameterization and the Carbon Bond 05 (CB05) combined with AERO5 for gas-phase and aerosol chemistry (summarized in Table 1). Anthropogenic emission inventories were obtained from MEIC as aforementioned. Natural emissions including BVOCs and NO were calculated offline using the Model of Emissions of Gases and Aerosols from Nature (MEGAN v2.10, Guenther, 2007).

We used WRF-CMAQ to investigate NO_x abatement on O_3 sensitivity during O_3 season, namely, August, when O_3 pollution gets extremely frequent throughout the country (Ding et al., 2008; Ding et al., 2013a; 2016; Wang et al., 2017). Here, we studied O_3 sensitivity regime in 2012 and 2016 since these two years featured NO_x emission peaks and a noticeable decrease in NO_x emissions (~25%), respectively. Two numerical experiments were designed, both of which shared exactly the same model configuration and input except for anthropogenic emissions. Sensitivity runs were conducted using the 2012-based and the 2016-based MEIC by reducing anthropogenic VOCs (AVOCs) or NO_x emissions, respectively. In this study, the O_3 sensitivity regime was identified in equivalent scenarios with 50% reductions in AVOCs and in NO_x emissions as suggested by Sillman and West (2009). The results are discussed in Section 3.3. Moreover, the relative incremental reactivity (RIR), reflecting the relative change of O_3 formation rate response to perturbations in precursors was also calculated to verify method mentioned above in diagnosing O_3 sensitivity (Cardelino and Chameides, 1995). Usually, a larger positive RIR of NO_x (or VOCs) indicates a higher probability that O_3 production will be more sensitive to NO_x (or VOCs). The definition and verification using RIR are provided in the supplementary (S2).

Further, we conducted O_3 isopleth simulations in eastern China for better understanding of current O_3 sensitivity in eastern China, which could support effective emission-control policy making in the near future. Sensitivity simulations were conducted for 10 days (Aug 16–25) which covered both O_3 polluted and non-polluted days representing a general level of O_3 season in eastern China. Generally, scenario simulations were performed with reducing NO_x or AVOCs emissions by 0%, 25%, 50%, 75% or 100%, respectively. In particular, more intensive reduction scenarios were conducted within the range of 0% and 50% reduction of NO_x or AVOCs emissions, aiming to provide more detailed O_3 responses to precursor perturbations. As a result, we performed 40 cases as depicted in the scenario matrix (Fig. S2).

3. Result and discussion

3.1. NO_x control in China

During the past decade in China, the control of O_3 precursors was mainly focused on NO_x emissions while less emission control strategy has been implemented on VOCs. Fig. 2 summarized the major progress and milestone of NO_x emission abatement policies during the past decade in China. Generally, the whole period can be divided into two phases. The first phase (2005–2011) is characterized by dramatical increases in NO_x emissions. Statistical results showed that NO_x emissions in eastern China were 19.48 Mt. (million ton) in 2005 while the amount accelerated to 26.05 Mt. (1.33 times higher) in 2010 (Zhao et al., 2013a, 2013b). Observations from satellite instruments also confirmed this increment with an increase rate of 5×10^{14} molecules/cm^2 per year in tropospheric NO_2 column between 2005 and 2011 (Fig. 1b). Indeed, the trend was similar with previous studies in eastern Asia (Itahashi et al., 2014; Richter et al., 2005; Irie et al., 2016;). The increment could be attributed to that, on one hand, NO_x emissions control within this period merely considered automobiles and power plants, the emission standards were relatively comfortable with GB13223-2003 for power plants and China III standard for vehicles (Fig. 1a). On the other hand, there had been a noticeable increase in newly-built power plants and vehicle populations, which turned up by 195% and 300%, respectively, according to Wang and Hao (2012). Consistently, Richter et al. (2005) and Itahashi et al. (2014) also attributed the NO_x increase to the rapid expansion of anthropogenic emissions.

Since the year of 2012, Chinese government has taken more ambitious steps to control NO_x emissions. Specifically, the 12th Five Year Plan (FYP) pledged to reduce the total NO_x emissions in China by 10% between 2010 and 2015, which for the first time set the target for NO_x control in China. In addition, a more tightened standard (GB13223-2011) has been put into force for NO_x emissions in power plants since 2012. The limit value of NO_x emissions was strengthened to be 100 mg/m^3 compared to the value of 450–1100 mg/m^3 based on the previous standard (GB13223-2003). In 2013, the State Council issued "Air Pollution Prevention and Action Plan" (APPAP), symbolizing the campaign entered into a more aggressive state. The plan aimed to reduce 25%, 20% and 15% $PM_{2.5}$ in JJJ, YRD and PRD between 2012 and 2017, respectively. As one pollutant co-emitting with primary particle and also one major precursor of $PM_{2.5}$, NO_x emissions would be inevitably substantially reduced. Stringent control measures included phasing out high-emitting industries, closing small/outdated factories, eliminating yellow label car, tightening industrial emission standard, improving fuel quality, introducing new efficient denitration technology, and etc. (Fig. 2a). Furthermore, ultra-low emission standard was initiated for large power plants since 2016, with a strict NO_x emission limit of 50 mg/m^3. Therefore, China's NO_x emissions were reduced by 23% during 2012–2016, in which emission reduction from power plant was the dominate contributor (Fig. 3). Accordingly, tropospheric NO_2 column concentrations in the second phase (2012–2016) decreased by ~31%, with the decreasing rate of -6×10^{14} molecules/cm^2 per year (Fig. 2b).

Such a great decline in NO_x emission led to the fact that ambient NO_2 concentrations decreased by 11.4% from 2013 to 2016 across China (Fig. 4), according to the monitoring data in major cities (National Bureau of Statistics of China, available at http://www.stats.gov.cn/tjsj/ndsj/, last access on Jan. 11, 2019). However, as another important O_3 precures, VOCs emissions slightly increased since 2008 due mainly to the lack of emission control in China, as demonstrated in Fig. 3. Noteworthy, accompanied with the decrease in ambient NO_x, O_3 concentrations showed an opposite trend, from 139 μg/m^3 in 2013 to 167 μg/m^3 in 2017. The aggravating O_3 pollution also holds true for JJJ, YRD and PRD regions (Fig. 4a-c), correspondence to increasingly serve photochemical pollution across China (Shao et al., 2009a; Ding et al., 2013a; Ma et al., 2016; Sun et al., 2016; Ding et al., 2017; Wang et al., 2017;).

3.2. Responses of O_3 to NO_x/VOCs emission reductions

The aforementioned drop in China's NO_x emission during 2012–2016 is expected to modify O_3 formation regime, and hence we performed sensitivity simulations to investigate the response of O_3. We firstly present the evaluation of WRF-CMAQ model. Hourly observed data collected from CMA (temperature, RH and wind) and CEMC (trace gases) were used to compare with those simulated. As

Table 1
Configuration and settings of WRF-CMAQ modeling system.

Item	Domain1	Domain2
Number of girds	170,130	199, 256
Horizontal resolution	36 km	12 km
Microphysics	WRF single-moment 5-class microphysics	
Short-wave radiation	Goddard	
Long-wave radiation	RRTM	
Meteorological observation nudging	Yes	
Boundary layer	ACM2	
Gas-phase chemistry	CB05	
Aerosol option	AERO5	
Anthropogenic emissions	MEIC	
Natural emissions	MEGAN	

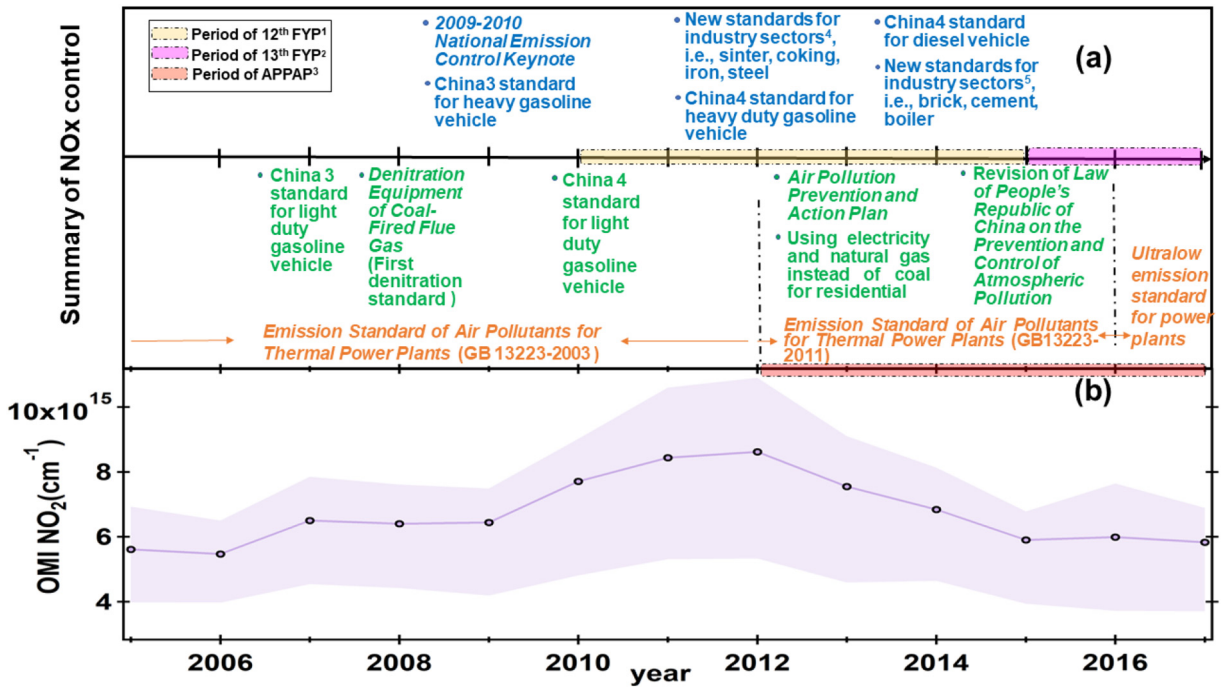

Fig. 2. Timeline summarizing major NO_x emission control strategies in China [1] The 12th Five Year Plan (2010–2015), a national goal set to reduce 10% national NOx emission with a result of 18.6% reductions in national NOx emissions. [2] The 13th Five Year Plan (2016–2020), a national goal set to reduce 15% national NOx emission, in progress. [3] Air Pollution Prevention and Action Plan (2012–2017), aimed to reduce 25%, 20% and 15% $PM_{2.5}$ in JJJ, YRD and PRD, respectively. [4] New standards for industrial sectors including sinter (GB28662-2012), coking (GB16171-2012), iron (GB28663-2012) and steel (GB28664-2012) [5] New standards for industrial sectors including brick (GB29620-2013), cement (GB4915-2013) and boiler (GB13271-2014).

summarized in Table 2, statistical calculations, including mean values (Obs_{mean} and Sim_{mean}), mean bias (MB), normalized mean bias (NMB), normalized mean error (NME), root mean square error (RMSE), and the index of agreement (IOA), were introduced for validations. It was indicated that all the meteorological parameters showed high values of IOA (Table 2) in JJJ, YRD and PRD, respectively, indicating the good correlation between observations and simulations. Meanwhile, the magnitudes were also well matched as the biases

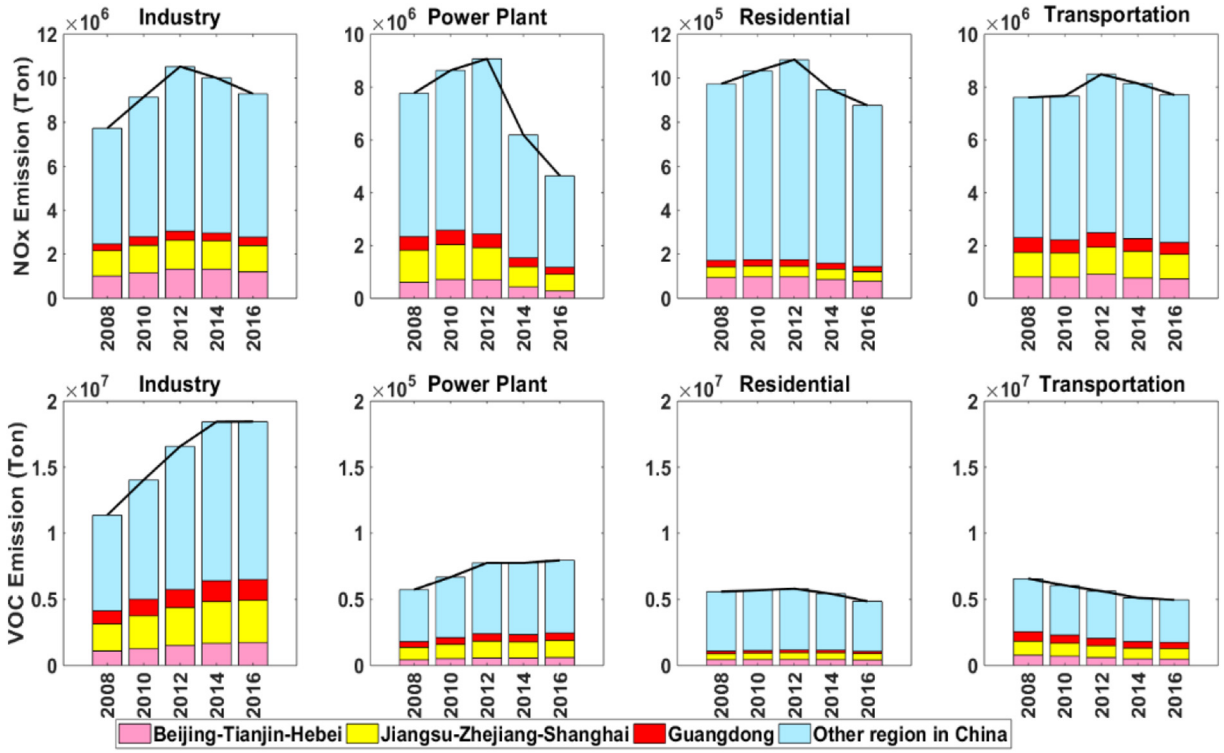

Fig. 3. NO_x and anthropogenic VOCs emissions from industry, power plant, residential and transportation from 2008 to 2016 in China*. *Emission data were obtained from MEIC (Multi-resolution emission inventory for China, http://www.meicmodel.org/).

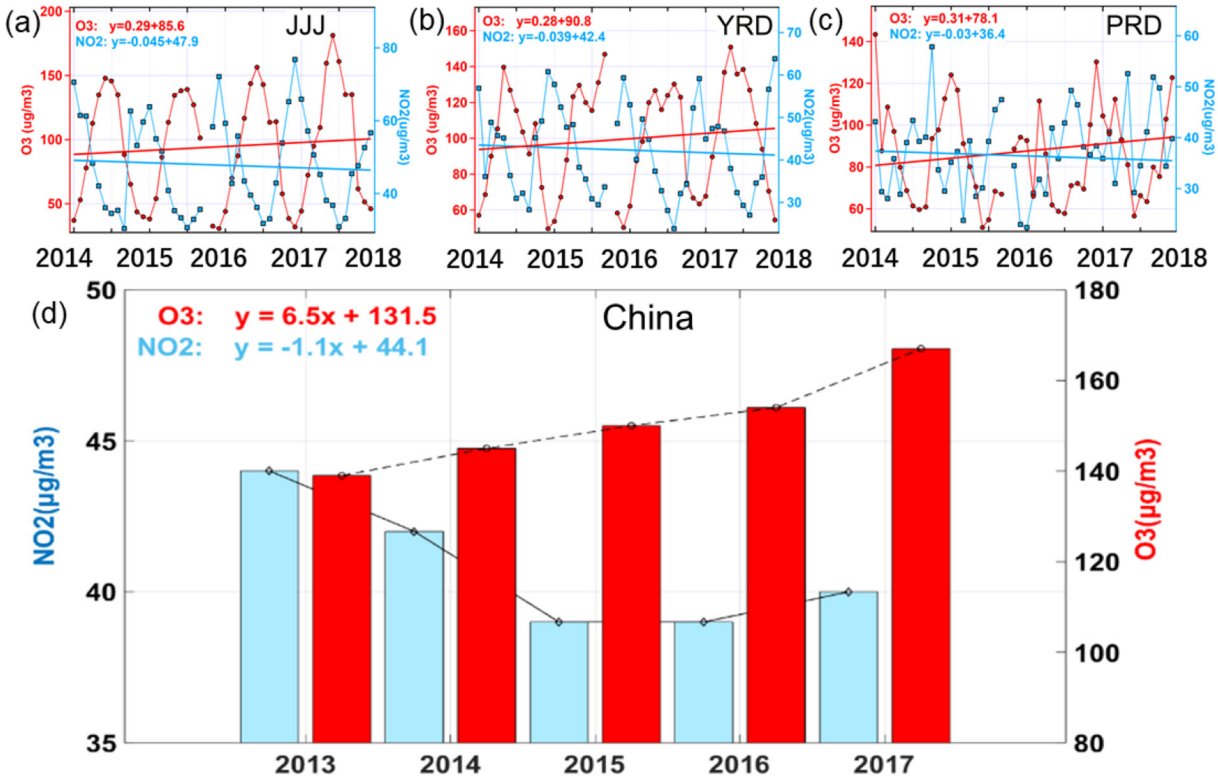

Fig. 4. Variations of surface monitored O_3 and NO_2 in JJJ (a), YRD (b), PRD (c) and whole China (d).

were relatively small (i.e., NMB, NME and RMSE). Therefore, the simulated weather conditions were well reproduced.

Simulated O_3 and NO_2 (Table 2) were also verified with field measurements. The mean bias of O_3 in JJJ, YRD and PRD were 5.2 ppb, −8.0 ppb and 5.8 ppb with IOA value equaled 0.84, 0.86 and 0.87, respectively, showing good model performance of reproducing O_3 concentrations. The simulations of NO_2 were slightly overestimated with MB of 5.2, 13.6 and 18.7 in JJJ, YRD and PRD, respectively. One possible reason was that NO_2 could be directly affected by local emissions in urbans, i.e., mobile vehicles, and such sources were a weakness of emission inventories. Besides, the finest horizontal resolution of 12 km × 12 km made it was difficult to reflect the topographic-induced effects which might affect air pollutants (Jiang et al., 2010; Li et al., 2013a, 2013b; Wang et al., 2015). Moreover, spatial comparisons of monthly O_3 (daily maximum) and NO_2 between simulation and observation were provided in Fig. S1. The comparisons showed that the modeled spatial distributions were consistent with those observed in eastern China. Since the aim of the study is to reflect general conditions based on monthly scales, reasonably well simulations of the trends and magnitudes could meet the objective. (Ding et al., 2004; Huang et al., 2005; Jiang et al., 2008; Li et al., 2013a, 2013b; Huang et al., 2016; Li et al., 2018; Wang et al., 2018a).

Table 2
Statistical comparisons of simulated and observed parameters.

Region	Parameter	Obs_{mean}	Sim_{mean}	MB	NMB	NME	RMSE	IOA
JJJ	T (°C)	25.9	25.2	−0.74	−0.02	0.06	2.14	0.92
	RH (%)	75.1	73.3	−1.75	−0.02	0.11	10.60	0.89
	WS (m/s)	1.9	2.8	0.9	0.57	0.71	1.53	0.61
	O_3 (ppb)	34.1	33.2	−0.9	−0.01	0.45	19.4	0.84
	NO_2 (ppb)	13.0	18.2	5.2	0.38	0.7	12.7	0.63
YRD	T (°C)	29.3	28.5	−0.8	−0.03	0.05	2.06	0.91
	RH (%)	74.8	79.6	4.8	0.06	0.11	10.16	0.86
	WS (m/s)	2.1	3.1	1.0	0.74	0.86	1.52	0.63
	O_3 (ppb)	39.5	31.5	−8.0	−0.22	0.46	0.84	0.86
	NO_2 (ppb)	14.1	27.7	13.6	1.16	1.06	19.2	0.52
PRD	T (°C)	28.7	29.0	0.2	0.01	0.04	1.63	0.91
	RH (%)	83.5	82.6	−0.9	−0.01	0.07	8.21	0.88
	WS (m/s)	2.2	3.1	0.9	0.46	0.65	1.78	0.69
	O_3 (ppb)	31.0	29.3	−1.7	−0.04	0.46	19.2	0.87
	NO_2 (ppb)	12.9	18.7	5.8	0.44	0.85	15.2	0.60

Fig. 5 shows the results of modeled O_3 using different year-based emission inventories under multi scenarios, namely, baselines, 30% and 50% reductions in NO_x and VOCs emissions in 2012 and 2016, respectively. By exploring the spatial distributions of O_3 in 2012 (Fig. 5a), relatively high levels of O_3 concentrations could be found in JJJ, YRD and PRD, with the monthly mean concentrations of 68 ppb, 69 ppb, and 61 ppb, respectively. When it came to 2016, regional mean concentration of O_3 in these three areas increased by 2.8 ppb, 3.7 ppb, and 4.1 ppb, respectively. The increments were consistent with the increasing trends of monitored O_3 in Fig. 4.

Fig. 5b gives O_3 response to 30% reduction of NO_x emissions for the year of 2012. As shown, despite slightly decreased O_3 level in some suburban and rural areas, most part of JJJ, YRD, and PRD underwent deteriorating O_3 pollution (mostly in urban areas), with the increment of 7.4%, 3.0% and 8.3% in JJJ, YRD, and PRD, respectively. Comparatively, O_3 concentration decreased approximately 10% in most of the rest eastern China, such as the central, the southwestern and the northwestern parts (defined as the rest areas hereafter). The responses became more obvious for the O_3 contrast in those urban areas and suburban/rural areas if NO_x emissions were reduced by 50% (Fig. 5c). For example, the maximum of O_3 increment was ~12 ppb (compared to that of ~9 ppb in 30% NO_x reduction scenario) and the minimum of O_3 decrease was ~5 ppb (compared to that of ~3 ppb in 30% NO_x reduction scenario) in some girds in JJJ. As a result, O_3 would increase by 6.4%, 2.0% ppb and 7.5% in JJJ, YRD and PRD, and decreased by 19.2% in the rest areas, respectively. Such responses implied that VOCs sensitivity controlled in most areas of the three developed city clusters, while NO_x sensitivity dominated in the rest areas.

In terms of 2016 when NO_x has been rigorously controlled, the increments of O_3 due to NO_x reductions shrank significantly in the three city

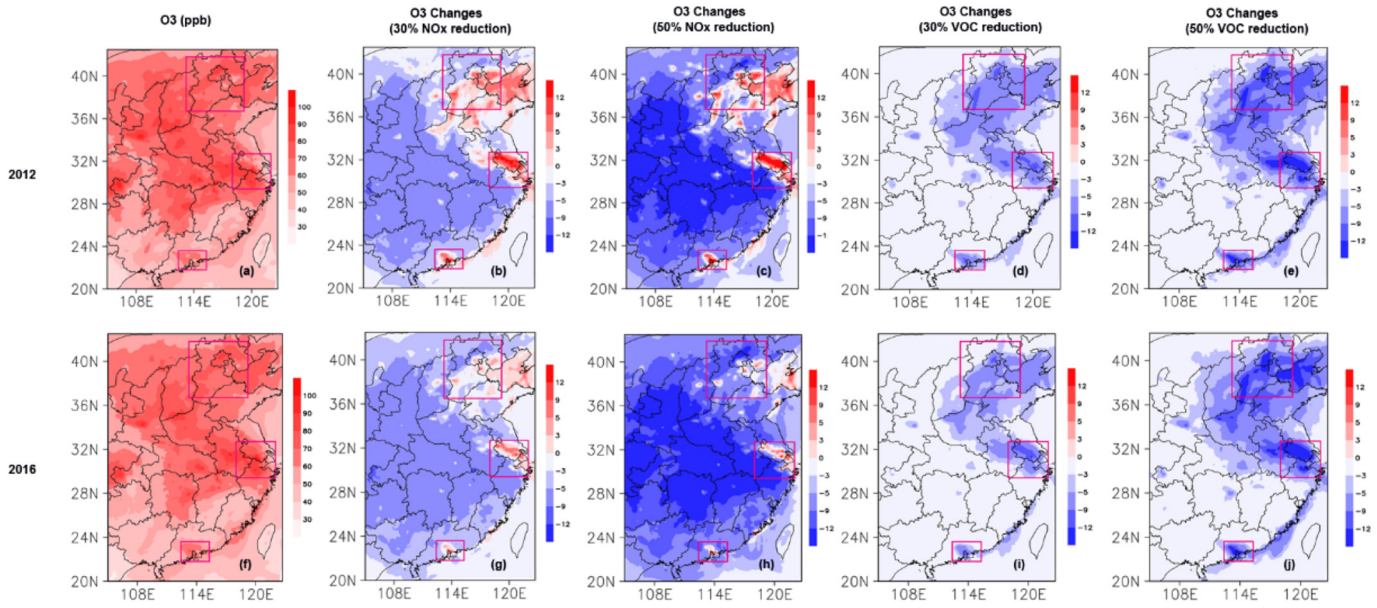

Fig. 5. Spatial distribution of max O_3 in 2012 and 2016 (a and f), respectively; O_3 changes due to perturbations of NO_x emissions (b, c, g, h) and VOCs emissions (d, e, i, j) in 2012 and 2016, respectively.

clusters (see red areas in Fig. 5g and Fig. 5h). The 2016-based 30% NO_x emission reduction scenario (Fig. 5g) showed that the increments of O_3 became weaker, with O_3 area mean (averaged O_3 concentration within a given region) changed by 1.1%, −1.4% and 0.5% in JJJ, YRD and PRD, respectively. The increments became more noticeable in the 2016-based 50% NO_x emission reduction scenario (Fig. 5h), with O_3 area mean changed by −3.2%, −8.2% and −4.5%, respectively. Such responses implied that O_3 formation sensitivities in these developed areas had somehow changed in 2016. When it came to O_3 responses to VOCs emissions, areas showed sensitive to VOCs emissions were North China Plain (including JJJ), YRD and PRD. In 2012, the 30% VOCs reduction scenario showed that O_3 decreased by 10.8%, 9.6%, and 12.0% in JJJ, YRD and PRD, respectively. And the decrease became 14.8%, 14.0% and 17.8% in terms of the 50% VOCs reduction scenario, respectively. Similar variations could also be found in 2016 (Fig. 5f and Fig. 5j), indicating that these areas were VOCs sensitive or at least mixed-sensitive. However, the rest areas showed little sensitive to VOCs emission perturbations with changes in O_3 concentration less than 2 ppb under all the VOCs reduction scenarios, which confirmed NO_x sensitive regime.

By considering O_3 responses to NO_x and VOCs emission reductions together, a common reducing area was found mainly located between 32°N-36°N of the east, implying a mix-sensitive area. Moreover, it is indicative of the transfer from a VOCs-sensitive dominated regime to a mix-sensitive dominated regime from 2012 to 2016 in JJJ, YRD and PRD, given the shrunken signals of O_3 rebounds due to NO_x emission reductions and the responses of O_3 to VOC emission perturbations as well.

3.3. Transition of O_3-NO_x-VOCs sensitivity regime

In order to quantitatively identify the effect of NO_x emission abatement on O_3-NO_x-VOCs sensitivity in eastern China, the method proposed by Sillman and West (2009) were taken. Locations of O_3 sensitivity were classified to NO_x sensitive, VOC sensitive, mixed sensitive, NO_x titration and no sensitive regimes. Specifically, NO_x sensitive (VOCs sensitive) regime was defined if O_3 decreases at least 5 ppb because of reducing NO_x emissions (VOCs emissions) and the decrease of O_3 due to NO_x emission reductions (VOCs emission reductions) is at least twice as large as the decrease due to reduced VOCs emissions (NO_x emissions). A place is identified as mixed sensitive regime if O_3 declines by more than 5 ppb in response to either reducing VOCs or NOx emissions and the reduction of O_3 due to VOCs emission reductions and NOx emission reductions differ by less than a factor of two. A site is controlled by NO_x titration if the O_3 increments are over 5 ppb due to NO_x emission reduction and O_3 decreases less than 5 ppb due to VOC emission reductions. Finally, a site is considered to be no sensitive regime if O_3 decreases less than 5 ppb in response to either VOCs emission or NO_x emission reductions. Furthermore, an additional method using RIR of NO_x (VOCs) emissions was also introduced to evaluate the results. The comparisons were provided in FigS3. The diagnosed patterns agreed well with each other indicating a convincible result.

3.3.1. Spatial pattern: enlarged mixed-sensitivity regime

Comparison of O_3 sensitivities between 2012 and 2016 is indicative of noticeable changes from VOCs sensitive regimes to mixed sensitive regimes in JJJ, YRD and PRD (Fig. 6). In 2012, widespread VOCs sensitive regimes were found over the three regions, and NO_x sensitive regimes were dominated in the rest areas. In terms of 2016, however, mixed sensitive regimes seemed to draw equal with VOCs sensitive regimes or even dominated in the three regions. Besides, similar changes were also observed in Shandong province, a part of North China Plain. In JJJ, the percentage of total grids occupied by VOC sensitive regime reduced from 62.8% in 2012 to 39.9% in 2016 whereas that of the mixed sensitive increased from 25.0% in 2012 to 46.2% in 2016 (Table 3). Though the percentages of VOCs sensitive regimes were shrunken in 2016, VOC sensitive regimes were still found in central Beijing, Tianjin, Tangshan and some other cities in Hebei Province. These cities are characterized by relatively high NO_x emissions likely from mobile vehicles or power plants. In YRD, the percentage of mixed sensitive regime increased from 32.4% in 2012 to 51.4% in 2016 (Table 3). In particular, mixed sensitive regimes were seen in cities such as Hangzhou, Nantong, Ningbo, Jiaxing and other cities in Zhejiang province after NO_x emission abatements. However, VOC sensitive regimes were still found in some developed urban cities, such as Shanghai, Suzhou, Wuxi, most of Nanjing and other cities in Jiangsu Province. Moreover, a few grids indicating NO_x titration occurred in 2012 disappeared in 2016. Usually, areas featuring high NO_x emissions sources are likely to be identified as NO_x titration regimes. The disappearances of NO_x titration regimes mostly concentrated in YRD region. In PRD, the 2016-year pattern demonstrated that both VOCs sensitive regime (20.9%) and mixed sensitive regime (50.0%) controlled in Guangzhou, Shenzhen, Dongguan and Foshan, while NO_x sensitive regimes dominated in rest cities of PRD (Fig. 6 and Table 3). Moreover, clear differences were also found in those

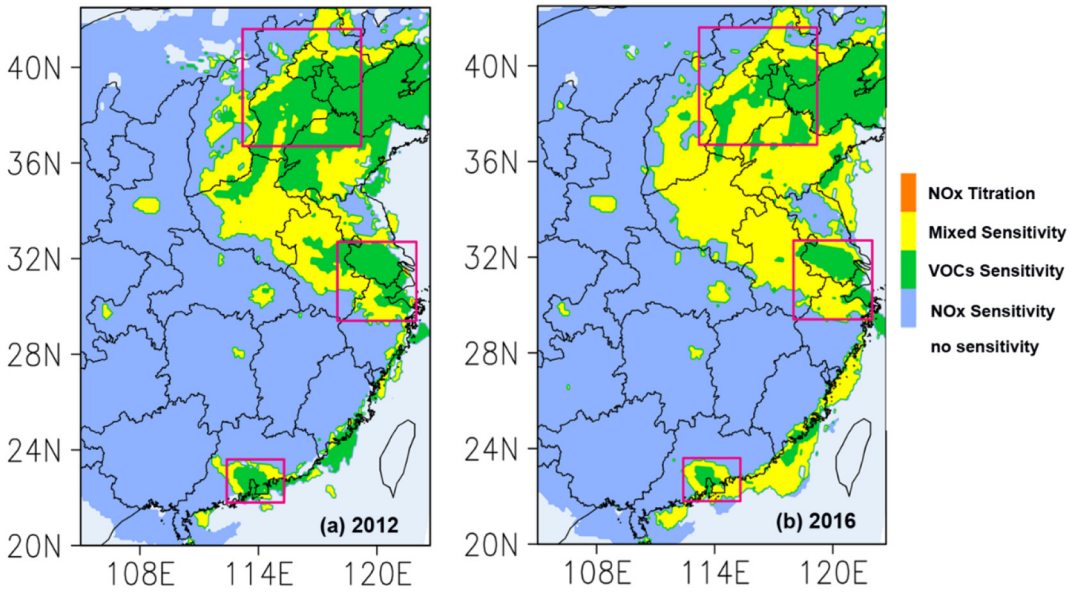

Fig. 6. Spatial comparison of O_3-NO_x-VOCs sensitive regime between 2012 and 2016 in eastern China.

marine areas, such as coastlines and Bohai. Since the study didn't incorporate any marine emissions, these areas were receptors of downwind areas which can only reflect O_3 sensitivity due to transport. O_3 sensitivities in most of these areas were also changed from VOCs sensitive regimes to mixed sensitive regimes.

Previous O_3-NO_x-VOCs sensitivity studies based on multiple approaches (in-situ observations, satellite retrievals and modellings) and were summarized and introduced to compare with our results (Table 4). Generally, our diagnosed results matched well with those results in eastern China. Specifically, Jin and Holloway (2015) employed OMI observations ($HCHO/NO_2$) to split O_3 sensitivity and found that transitional regimes (mixed sensitive) dominated in most areas of JJJ, YRD and PRD, respectively, whereas we found both VOCs sensitivity and mixed sensitivity were the dominated regimes. The discrepancy between the two studies can be attributed to the following aspects. One possible reason is that satellite measurements are based on optical properties which are affected by clouds, aerosols, precipitations, and surface reflectivity. The observation contains uncertainties itself. For example, the uncertainty of HCHO products range from ~30% to 40% according to De Smedt et al. (2010). Besides, satellite observations provide vertical column concentrations which are different to ground-level concentrations (Boersma et al., 2004). More importantly, our further analysis showed that O_3 sensitivities depicted diurnal changes in the three regions with a shift of VOCs sensitive in the morning to mixed or NO_x sensitive in the afternoon (details refer to Section 3.3.2). In fact, OMI observations only provide once-a-day observations and are limited to the early afternoon conditions (Jin and Holloway, 2015).

3.3.2. Diurnal variation: elevated O_3 production before noontime

In addition to transitions of O_3-NOx-VOCs sensitivity regime in spatial distribution, ozone production also displayed obvious changes in diurnal pattern. We compared the simulated net O_3 formation rate between 2012 and 2016 (Fig. 7). The net O_3 formation rate was calculated with the similar to Wang et al. (2018b), with the consideration of both O_3 production and O_3 destruction pathways. The reactions of $RO_2 + NO$ and $HO_2 + NO$, were treated as the pathways leading to O_3 formation, whereas O_3 destruction pathways included $O1D + H_2O$; $O_3 + HO_2$; $O_3 + OH$; $NO_2 + OH$; and $O_3 + VOCs$. The net O_3 formation rate was calculated by subtracting the O_3 destruction rate from O_3 production rate. In this study, the Integrated Reaction Rate (IRR) module incorporated in CMAQ was triggered to acquire the rates of the above gas-phase reactions.

It was found that peak O_3 formation rate was about 1.5–3 ppb/h higher in 2016 than that in 2012 regardless of region. The change was reasonable, as reduction of NO_x leads to O_3 increase in the VOC-limited regime which controlled O_3 formation in most areas of the three regions in 2012. Meanwhile, the NO_x emission control resulted in the shift of the peak net O_3 formation rate, which occurred about 1–1.5 h earlier in 2016 than that in 2012. This might also be related to the reduction of NO_x in recent years. With the consumption of NO_x in the daytime photochemical reactions, O_3 formation generally switch from the VOCs sensitive regime to the mixed sensitive regime or even NO_x sensitive regime (as discussed in Fig. 8). The NO_x emission controls in China may give rise to earlier peaks of the net O_3 formation because the mixed sensitive regime features the highest O_3 production rates compared to the VOCs (NO_x) sensitive regimes with the same NO_x or VOCs emissions.

Fig. 8 illustrated the diurnal variations of O_3 sensitivity in JJJ, YRD and PRD. All of the three regions showed similar diurnal variations. Before 8:00 am, O_3 was depleted via NO_x titration. As the boundary layer developed, O_3 formation tended to be VOCs sensitive in the morning. Since noon time (O_3 peak hours), mixed sensitive regimes and NO_x sensitive regimes dominate till the late afternoon. It was found PRD was more sensitive to NO_x emissions than the other two regions in the afternoon because of more efforts spent in historical emission control. Indeed, PRD has been playing a leading role in mitigating air quality throughout China and the effective control of NO_x emissions could be traced back to 2003 due to the joint efforts of Guangdong and Hong Kong governments (Zhong et al., 2013; Wang et al., 2017). Similar with the report from other locations (Kleinman, 2005; Sillman and West, 2009), the diurnal transitions from the dominance of VOCs sensitive regimes in the morning to the mixed sensitive (and NO_x sensitive in PRD) regimes in the afternoon were likely due to photochemical consumption of NO_x and

Table 3
Comparisons of model grid proportions of O_3 sensitivity regime in JJJ, YRD and PRD between 2012 and 2016 (unit: %).

	VOC-sensitive		NOx-sensitive		Mix-sensitive		NOx titration	
	2012	2016	2012	2016	2012	2016	2012	2016
JJJ	62.8	39.9	12.2	13.9	25	46.2	~0	~0
YRD	54.9	35.9	11.2	12.5	32.4	51.4	1.5	0.2
PRD	50.8	20.9	18.3	29.1	30.9	50	~0	~0

Table 4
Comparisons with previous O_3 sensitivity studies.

Study area	Site info	Study time	Method	O_3 sensitivity	References	This study
Beijing	Birds Nest, urban;	07–092008; 08.2014;	△Ox/△NOz; VOC/O_3;	VOC-limited; VOC-limited;	Sun et al. (2011) Shao et al., (2009a)	VOC-limited in central areas and mixed-limited in suburban/rural
	PKU (urban); Urban and rural; Whole area;	07.2005; 2013 Summer;	CMAQ-RSM; Satellite retrievals;	Urban: VOC-limited, Rural: NOx-limited; Mixed-limited in most area	Xing et al. (2011) Jin and Holloway (2015)	
Tianjin	Urban;	07–082010;	NCAR_MM;	Mix-limited;	Ran et al. (2012)	VOC-limited dominated
JJJ	Whole area	2015	CMAQ-ISAM;	VOC-limited in urban and mixed/NOx-limited in suburban/remote;	Han et al. (2018)	VOC-limited in urbans and mixed-limited in suburban/rural
	Whole area	2013 Summer	Satellite retrievals (HCHO/NO2)	Transitional dominated	Jin and Holloway (2015)	
Nanjing	SORPES (suburban);	2011–2012; 10. 2014;	△O_3/△NOy; OBM (MCM);	VOC-limited; VOC-limited;	Ding et al. (2013a) Xu et al. (2017)	VOC-limited dominated
	SORPES (suburban); Four urban sites	06–082013;	OBM (CB4);	VOC-limited;	An et al. (2013)	
Shanghai	Xujiahui (urban)	07–082009;	NCAR_MM;	NOx-inhibited;	Ran et al. (2012)	VOC-limited
	Urban	2006–2007; 09. 2009	NCAR_MM; WRF-Chem	VOC-limited; VOC-limited	Geng et al. (2008); Tie et al. (2009)	
	Urban Rural and urban	07. 2007	CMAQ;	Urban: VOCs-limited; Rural: NOx-limited	Li et al. (2011)	
Hefei	Whole area	2015–2017	Satellite retrievals;	NOx-limited;	Sun et al. (2019)	NOx-limited
YRD	Whole area	2013 Summer	Satellite retrievals (HCHO/NO2)	Transitional dominated	Jin and Holloway (2015)	VOCs-limited and mixed-limited dominated
Guangzhou	WQS (suburban)	10–122,007	OBM (MCM);	VOCs-limited	Cheng et al. (2010)	VOC-limited and mixed limited
	Urban	2000 2006	OBM; OBM(CB4);	VOCs-limited Urban: VOCs-limited	Shao et al. (2009a, 2009b)	
	Urban and suburban	Summer;		Suburban: NOx-limited	Lu et al. (2010)	
Zhuhai	Wanshan (suburban)	2013 Autumn	PBM-MCM	Transitional (Mixed)	Wang et al. (2018b)	Mixed limited;
PRD	Whole area	2012	CMAQ	Urban: VOCs-limited Remote: NOx-limited	Wang et al. (2017)	Urban: VOCs-limited and mixed limited; Remote: NOx-limited
	Whole area	2013 Summer	Satellite retrievals (HCHO/NO2)	Transitional dominated	Jin and Holloway (2015)	

increased vertical dilution. Lei et al. (2008) also associated the transition with photochemical aging in the plume downwind from source regions.

Such diurnal variations indicated that the O_3 sensitivity of a certain site at a given hour do not apply to other times, which was true with those satellite studies. For example, Tang et al. (2012) used the ratio of HCHO/NO_2 from GOME observations and concluded that North China Plain was sensitive to VOCs whereas Jin et al. (2017) suggested the dominance of mixed sensitive regimes and NO_x sensitive regimes by taking advantage of the same ratio but from OMI observations. The discrepancy was due to that the crossing time of GOME was about 10:00 local time (LT) in the morning whereas OMI crossed at around 14:00 LT in the afternoon. Fig. 8d-i showed model grids sorted by precursor sensitivities at the crossing time of GOME and OMI, namely, 10:00 and 14:00 (LT), respectively. All the three regions depicted the clear variations with a majority of model grids sensitive to VOCs at 10:00 LT (taking up 65%, 61% and 73% of JJJ, YRD and PRD, respectively) whereas mixed sensitive regimes dominating at 14:00 LT in the afternoon. The diurnal characteristics of O_3-NO_x-VOCs sensitivity indicated that controlling VOCs emissions was instructive for reducing the overall O_3 mixing ratio and O_3 did also benefit from NO_x control if somehow NO_x emissions could be reduced only in the afternoon.

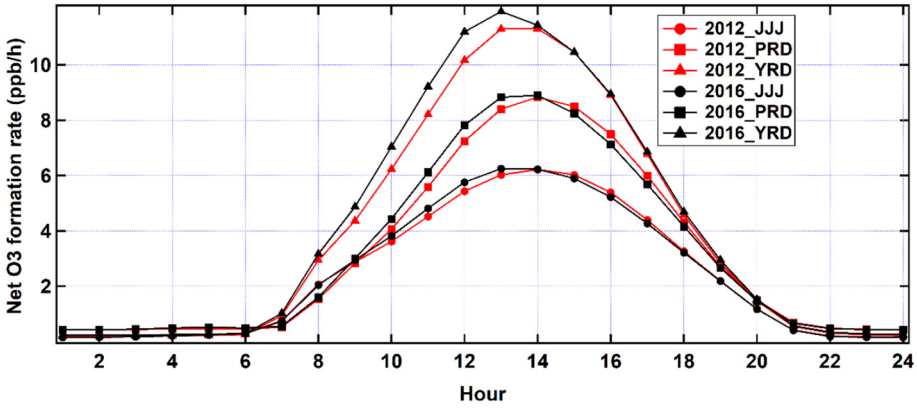

Fig. 7. Comparison of O_3 net formation rate. (Net O_3 rate[1*] is calculated using O_3 production rate[2*] to minus O_3 destruction rate[3*]) [1*]Net O_3 rate = production rate – destruction rate; [2*]production rate considers pathways of: RO_2 + NO; HO_2 + NO; [3*]destruction considers pathways of: O1D + H_2O; O_3 + HO_2; O_3 + OH; NO_2 + OH; O_3 + VOCs.

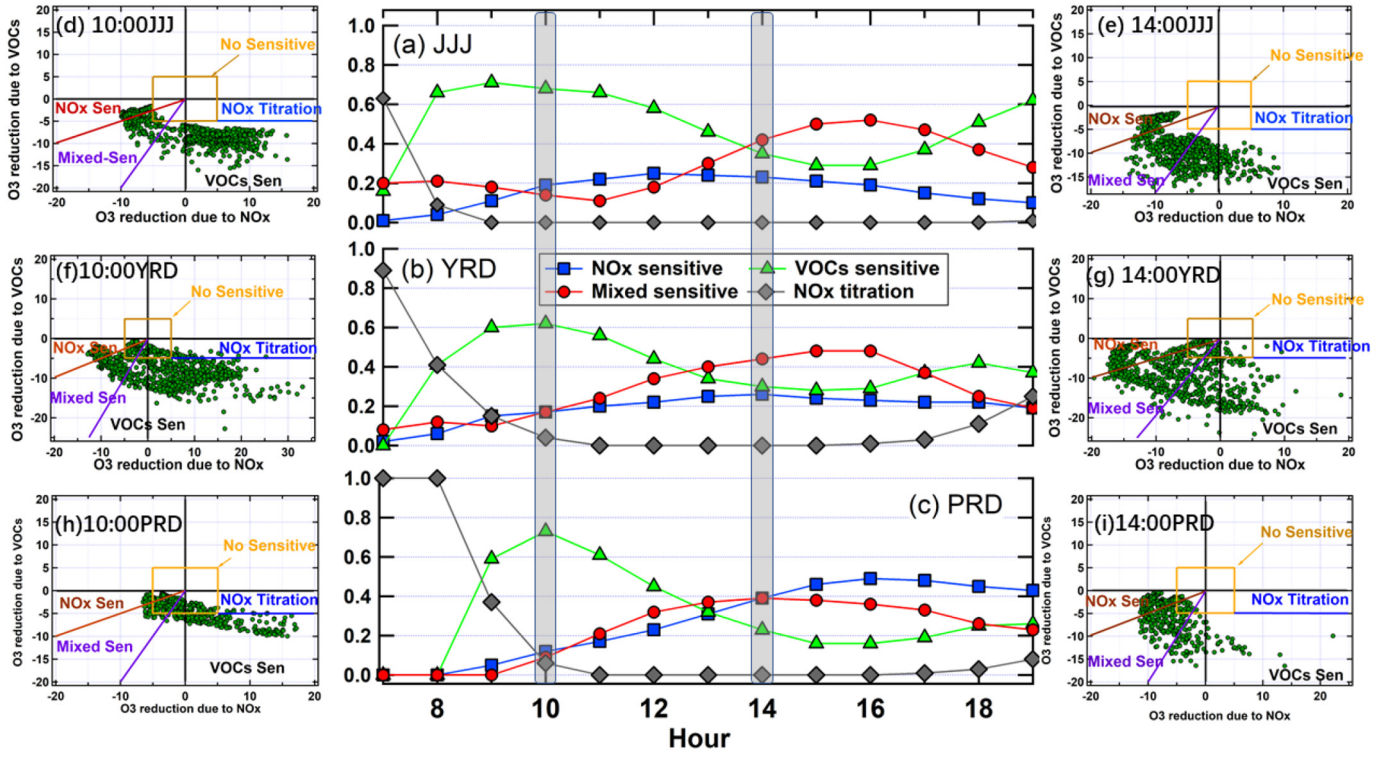

Fig. 8. Percentages of O_3-NOx-VOCs sensitive regime in 3 regions from 07: am to 19:00 pm (a-c). The grey shades highlight crossing time of GOME and OMI at 10:00 am and 14:00 pm (LT), respectively. Model grids sorted by precursor sensitivity at 10:00 am and 14:00 pm (d-i) in 3 regions.

3.4. Implications for O_3 mitigation

The relationships of O_3, NOx and VOCs are shown in Fig. 9. In this study, the O_3 isopleth was achieved by using linear regressions from 40 scenarios based on 10-day simulations (Aug 16–25). The selected periods covered both non O_3 polluted days and O_3 polluted days, thus could be regarded as general conditions in JJJ, YRD and PRD, respectively. In Fig. 10, the VOCs sensitive, mixed sensitive and NO_x sensitive regimes, corresponded to the maximum 1-hour O_3 concentration for given precursors, were separated by ridge lines (Ou et al., 2016). To be noted that the base scenarios were at the upper right corner (red dots) and represented the benchmarks without any NO_x or VOCs emission reductions. It could be found that all the base scenarios in YRD and PRD were within the area of the mixed sensitive regimes, indicating that O_3 formation was sensitive to both VOCs and NO_x. In JJJ, the base scenario was above the ridge line, suggesting that VOCs sensitive regime dominated, while it was not far away from the mixed sensitive regime. Though the O_3 isopleths were based on 10-day simulations, the results of base scenarios were generally consistent with the monthly analyses in Fig. 6, further confirming the convincible results.

Another important finding in Fig. 9 (a-c) is that relatively high O_3 mixing ratios concentrated within the regions of mixed sensitive regimes in all of the 3 regions, correspondence to continuously increasing O_3 levels monitored in recent year. In fact, a nationwide control against NOx emissions has been taken steps while VOCs emission controls are ignored in the past. This means that developed regions, particularly JJJ, YRD and PRD in eastern China, are suffering from VOCs sensitive regimes to the high-O_3-level mixed sensitive regimes. Suppose past

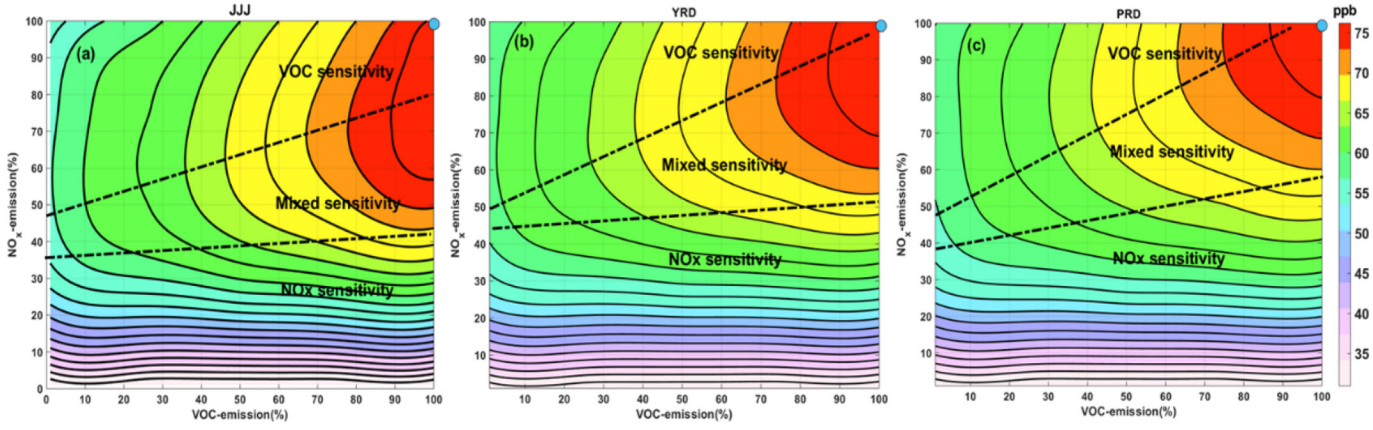

Fig. 9. O_3 isopleth in JJJ, YRD and PRD, respectively.

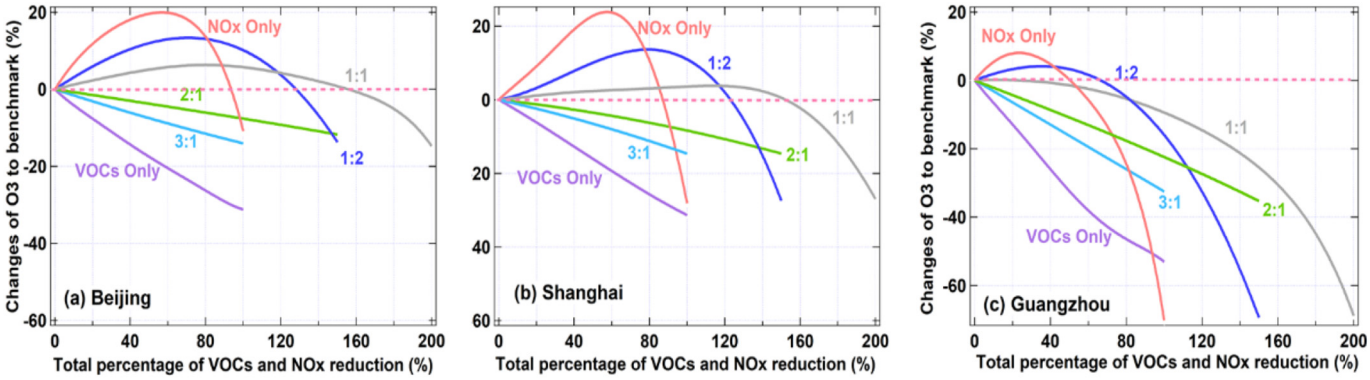

Fig. 10. Changes of O_3 due to different reduction of AVOC/NOx in Beijing (a), Shanghai (b) and Guangzhou (c).

control tendency is maintained in the future (NO_x control only), China would experience a time suffering from high O_3 mixing ratio as the band of mixed sensitive regime is rather wide. However, if VOCs emissions could be somehow controlled, the band of mixed sensitive regime tends to be narrower. Therefore, to provide scientific support for future emission control strategy, we further explore the co-benefit based on NO_x and VOCs reductions.

Three typical cities, Beijing, Shanghai and Guangzhou, within the 3 regions were selected to study the changes of O_3 to different degrees of precursor reductions (Fig. 10a-b). Two sets of reduction schemes were considered including the NO_x-targeted and the VOCs-targeted reductions. Generally, the NO_x-targeted (VOCs-targeted) reductions referred to scenarios with major controls on NO_x (VOCs) emissions, which covered 3 scenarios with only reducing NO_x (VOCs) emissions (The NO_x [VOCs] Only) and with AVOC/NO_x reduction ratio equaled to 1:1 (3,1) and 1:2 (2,1), respectively. The horizontal axis in Fig. 10a-b referred to the total reduction percentage of combined NO_x and AVOCs emissions. For example, a reduction of 120% emissions in the horizontal axis indicated that 120% reduction of NO_x and VOCs emissions with AVOC/NO_x equaled to 3:1, 2:1, 1:1 or 1:2, or with only 120% NO_x emissions reduction, or with only 120% VOCs emissions reduction, respectively.

The NO_x Only scenario could be generally regarded as China's past control strategy as VOCs control was almost neglected. Under the NO_x Only scenario, NO_x disbenefits could be found in all the 3 cities with different degrees of O_3 increments. The O_3 decreases were not practical as it required dramatical reduction of NO_x emissions, for example, more than ~85% for Beijing and Shanghai and more than ~45% for Guangzhou. Considering the fact that China has spent five years (2012–2016) to reduce ~25% NO_x emissions, it would take another 3 five-year periods for Beijing and Shanghai and 1 five-year period for Guangzhou to achieve O_3 decrease if simply following past control tendency. This implied that controlling NO_x emissions would degrade air quality with O_3 increments at least in the short-term (for Guangzhou) or even in the long-term (for Beijing and Shanghai). Similar responses could be found for the other two NOx-targeted scenarios (with the AVOC/NO_x = 1:2 and 1:1). Different from Beijing and Shanghai, the benefit of O_3 decrease in Guangzhou could be met with relatively less efforts for those NO_x-targeted scenarios, especially for the 1:1 scenario, of which O_3 increments were not seen. This implied that the future O_3 control in PRD was somehow more feasible than in JJJ and YRD. Furthermore, it became more promising in terms of those VOCs-targeted controls. All the three cities demonstrated various degrees of O_3 reduction. The VOCs Only received the most rapidly O_3 decrease, followed by the 3:1 scenario and the 2:1 scenario, respectively. Comparing to the disbenefits in NO_x-targeted control, the VOCs-targeted was more feasible and practical. Hence, it is strongly suggested that governments take VOCs-targeted control in the future.

4. Summary and conclusions

China has been suffering from increasing O_3 pollution associated with a notable drop of NO_x during the past five years. Since that O_3 pollution has close but nonlinear relationships with NO_x and VOCs emission intensity, recent dramatic controls on NO_x emissions in China were expected to pose significant perturbations on the sensitivity of O_3 production. To shed more light on the current situation of O_3 pollution and get more in-depth understandings on how to scientifically control NO_x emissions and VOCs emissions spatially and temporally, we integrated continuous satellite retrievals, ground-based measurements together with modeling approaches in this study.

Statistical data revealed that NO_x emissions decreased by ~ 25% from 2012 to 2016, corresponding to a noticeable drop in tropospheric NO_2 column concentrations in eastern China (~ 30%). The effective NO_x abatement was due to the stringent emission control measures represented by the nationwide policy plans like FYP and APPAP. However, monitored O_3 mixing ratios have increased and are about 20.1% higher in 2017 than in 2013 (rising rate = 6.5 μg/m^3/year), suggesting O_3 pollution is becoming more stringent even though NO_x emissions are reduced.

A regional chemical transport model, WRF-CMAQ, was employed to explore the variations and characteristics of O_3-NO_x-VOCs sensitivities in eastern China with a special focus on developed regions such as JJJ, YRD and PRD. In spatial, all the regions demonstrated the change of the dominance of the VOCs sensitive regime to the mixed sensitive regime in O_3 formation. Total grids occupied by mixed sensitive regimes in JJJ, YRD and PRD increased from 25.0%, 31.4% and 30.1% in 2012 to 42.1%, 52.2% and 50.4% in 2016, respectively, indicating the overall increasing sensitivity to NO_x. In temporal, a diurnal shift of O_3 sensitivity existed in all the three regions with VOCs sensitive regimes dominated in the morning shifting to mixed sensitive dominated regimes in the afternoon. Due to the transition in O_3-NO_x-VOCs sensitivity, the diurnal peak of net O_3 formation rate was ~1–1.5 h earlier in 2016 compared to 2012.

We further conducted O_3 isopleth studies to explore the possible way for effective O_3 mitigation. It is suggested that past control measures that only focused on NO_x aggravate O_3 pollution. On the contrary, O_3 drop could be found among the three regions with the reduction ratio of AVOCs/NO_x more than 2:1, indicating that VOCs-targeted control is more practical and feasible for O_3 pollution mitigation in eastern China.

Acknowledgement

This work was supported by the Ministry of Science and Technology of the People's Republic of China (2018YFC0213800, 2016YFC0200500) and the National Natural Science Foundation of China (91544231, 41805131, 41725020, 91744311 and 41505109).

Appendix A. Supplementary data

Supplementary data to this article can be found online at https://doi.org/10.1016/j.scitotenv.2019.04.388.

References

An, J., Zou, J., Wang, J., Lin, X., Zhu, B., 2015. Differences in ozone photochemical characteristics between the megacity Nanjing and its suburban surroundings, Yangtze River Delta, China. Environ. Sci. Pollut. Res. 22 (24), 19607–19617.

Atkinson, R., 2000. Atmospheric chemistry of VOCs and NOx. Atmos. Environ. 34, 2063–2101.

Boersma, K.F., Eskes, H.J., Brinksma, E.J., 2004. Error analysis for tropospheric NO2 retrieval from space. J. Geophys. Res.-Atmos. 109.

Boersma, K.F., Eskes, H.J., Veefkind, J.P., Brinksma, E.J., van der, A.R.J., Sneep, M., et al., 2007. Near-real time retrieval of tropospheric NO2 from OMI. Atmos. Chem. Phys. 7, 2103–2118.

Boersma, K.F., Eskes, H.J., Dirksen, R.J., van der, A.R.J., Veefkind, J.P., Stammes, P., et al., 2011. An improved tropospheric NO2 column retrieval algorithm for the Ozone Monitoring Instrument. Atmos. Meas. Tech. 4, 1905–1928.

Booker, F., Muntifering, R., McGrath, M., Burkey, K., Decoteau, D., Fiscus, E., et al., 2009. The ozone component of global change: potential effects on agricultural and horticultural plant yield, product quality and interactions with invasive species. J. Integr. Plant Biol. 51, 337–351.

Brauer, M., Freedman, G., Frostad, J., van Donkelaar, A., Martin, R.V., Dentener, F., et al., 2016. Ambient air pollution exposure estimation for the global burden of disease 2013. Environ. Sci. Technol. 50, 79–88.

Cardelino, C.A., Chameides, W.L., 1995. An observation-based model for analyzingozone precursor relationships in the urban atmosphere. J. Air Waste Manage. Assoc. 45, 161e180.

Cheng, H.R., H., Guo, Saunders, S.M., Lam, S.H.M., Jiang, F., Wang, X.M., Wang, T.J., 2010. Assessing photochemical ozone formation in the Pearl River Delta with a photochemical trajectory model. Atmos. Environ. 44, 4199–4208. https://doi.org/10.1016/j.atmosenv.2010.07.019.

Chou, C.C.K., Tsai, C.Y., Shiu, C.J., Liu, S.C., Zhu, T., 2009. Measurement of NOy during campaign of air quality research in Beijing 2006 (CAREBeijing-2006): implications for the ozone production efficiency of NOx. J. Geophys. Res.-Atmos. 114.

De Smedt, I., Stavrakou, T., Müller, J.F., Van Roozendael, M., 2010. <De Smedt et al.pdf>. Geophys. Res. Lett. 37.

de_Richter, R., Caillol, S., 2011. Fighting global warming: the potential of photocatalysis against CO2, CH4, N2O, CFCs, tropospheric O3, BC and other major contributors to climate change. J Photochem Photobiol C: Photochem Rev 12, 1–19.

Ding, A., Wang, T., Zhao, M., Wang, T., Li, Z.K., 2004. Simulation of sea-land breezes and a discussion of their implications on the transport of air pollution during a multi-day ozone episode in the Pearl River Delta of China. Atmos. Environ. 38, 6737–6750.

Ding, A., Wang, T., Thouret, V., Cammas, J.-P., Nédélec, P., 2008. Tropospheric ozone climatology over Beijing: analysis of aircraft data from the MOZAIC program. Atmos. Chem. Phys. 8, 1–13.

Ding, A.J., Fu, C.B., Yang, X.Q., Sun, J.N., Petaja, T., Kerminen, V.M., et al., 2013a. Intense atmospheric pollution modifies weather: a case of mixed biomass burning with fossil fuel combustion pollution in eastern China. Atmos. Chem. Phys. 13, 10545–10554.

Ding, A.J., Fu, C.B., Yang, X.Q., Sun, J.N., Zheng, L.F., Xie, Y.N., et al., 2013b. Ozone and fine particle in the western Yangtze River Delta: an overview of 1 yr data at the SORPES station. Atmos. Chem. Phys. 13, 5813–5830.

Ding, A., Nie, W., Huang, X., Chi, X., Sun, J., Kerminen, V.-M., Xu, Z., Guo, W., Petaja, T., Yang, X., Kulmala, M., Fu, C., 2016. Long-term observation of air pollution-weather/climate interactions at the SORPES station: a review and outlook. Front. Environ. Sci. Eng. 10 (5), 15. https://doi.org/10.1007/s11783-016-0877-3.

Ding, A., Huang, X., Fu, C., 2017. Air pollution and weather interaction in East Asia. Oxford Research Encyclopedias: Environmental Science https://doi.org/10.1093/acrefore/9780199389414.013.536.

Fann, N., Lamson, A.D., Anenberg, S.C., Wesson, K., Risley, D., Hubbell, B.J., 2012. Estimating the national public health burden associated with exposure to ambient PM2.5 and ozone. Risk Anal. 32, 81–95.

Geng, F., Tie, X., Xu, J., Zhou, G., Peng, L., Gao, W., et al., 2008. Characterizations of ozone, NOx, and VOCs measured in Shanghai, China. Atmos. Environ. 42, 6873–6883.

Gilliland, A.B., Hogrefe, C., Pinder, R.W., et al., 2008. Dynamic evaluation of regional air quality models: assessing changes in O3 stemming from changes in emissions and meteorology[J]. Atmos. Environ. 42 (20), 5110–5123.

Guenther, A., 2007. Estimates of global terrestrial isoprene emissions using MEGAN (model of emissions of gases and aerosols from nature) (vol 6, pg 3181, 2006). Atmos. Chem. Phys. 7, 4327.

Han, X., Zhu, L., Wang, S., Meng, X., Zhang, M., Hu, J., 2018. Modeling study of impacts on surface ozone of regional transport and emissions reductions over North China Plain in summer 2015. Atmos. Chem. Phys. 18 (16), 12207–12221.

He, K.B., 2012. Multi-resolution emission inventory for China (MEIC): model framework and 1990–30 2010 anthropogenic emissions. International Global Atmospheric Chemistry Conference.

He, J., Gong, S., Yu, Y., Yu, L., Wu, L., Mao, H., et al., 2017. Air pollution characteristics and their relation to meteorological conditions during 2014-2015 in major Chinese cities. Environ. Pollut. 223, 484–496.

Huang, J.P., Fung, J.C.H., Lau, A.K.H., Qin, Y., 2005. Numerical simulation and process analysis of typhoon-related ozone episodes in Hong Kong. J. Geophys. Res.-Atmos. 110.

Huang, X., Zhou, L.X., Ding, A.J., Qi, X.M., Nie, W., Wang, M.H., et al., 2016. Comprehensive modelling study on observed new particle formation at the SORPES station in Nanjing, China. Atmos. Chem. Phys. 16, 2477–2492.

Huang, X., Wang, Z.L., Ding, A.J., 2018. Impact of aerosol-PBL interaction on haze pollution: multiyear observational evidences in North China. Geophys. Res. Lett. 45, 8596–8603.

Irie, H., Muto, T., Itahashi, S., et al., 2016. Turnaround of tropospheric nitrogen dioxide pollution trends in China, Japan, and South Korea[J]. Sola 12, 170–174.

Itahashi, S., Uno, I., Irie, H., et al., 2014. Regional modeling of tropospheric NO2 vertical column density over East Asia during the period 2000–2010: comparison with multisatellite observations. Atmos. Chem. Phys. 14 (7), 3623–3635.

Jiang, F., Wang, T.J., Wang, T.T., Xie, M., Zhao, H., 2008. Numerical modeling of a continuous photochemical pollution episode in Hong Kong using WRF-chem. Atmos. Environ. 42, 8717–8727.

Jiang, F., Guo, H., Wang, T.J., Cheng, H.R., Wang, X.M., Simpson, I.J., et al., 2010. An ozone episode in the Pearl River Delta: field observation and model simulation. J. Geophys. Res.-Atmos. 115.

Jin, X., Holloway, T., 2015. Spatial and temporal variability of ozone sensitivity over China observed from the ozone monitoring instrument. J. Geophys. Res.-Atmos. 120, 7229–7246.

Jin, X.M., Fiore, A.M., Murray, L.T., Valin, L.C., Lamsal, L.N., Duncan, B., et al., 2017. Evaluating a space-based Indicator of surface ozone-NOx-VOC sensitivity over midlatitude source regions and application to decadal trends. J. Geophys. Res.-Atmos. 122, 10231–10253.

Kleinman, L.I., 2005. The dependence of tropospheric ozone production rate on ozone precursors. Atmos. Environ. 39, 575–586.

Lei, W., Zavala, M., de Foy, B., Volkamer, R., Molina, L.T., 2008. Characterizing ozone production and response under different meteorological conditions in Mexico City. Atmos. Chem. Phys. 8, 7571–7581.

Levelt, P.F., van den Oord, G.H.J., Dobber, M.R., et al., 2006. The ozone monitoring instrument[J]. IEEE Trans. Geosci. Remote Sens. 44 (5), 1093–1101.

Li, L., Chen, C., Huang, C., et al., 2011. Ozone sensitivity analysis with the MM5-CMAQ modeling system for Shanghai[J]. J. Environ. Sci. 23 (7), 1150–1157.

Li, Y., Lau, A.K.H., Fung, J.C.H., Zheng, J., Liu, S., 2013a. Importance of NOx control for peak ozone reduction in the Pearl River Delta region. J. Geophys. Res.-Atmos. 118, 9428–9443.

Li, Y., Lau, A.K.H., Fung, J.C.H., Zheng, J.Y., Liu, S.C., 2013b. Importance of NOx control for peak ozone reduction in the Pearl River Delta region. J. Geophys. Res.-Atmos. 118, 9428–9443.

Li, Q., Zhang, L., Wang, T., Wang, Z., Fu, X., Zhang, Q., 2018. "New" reactive nitrogen chemistry reshapes the relationship of ozone to its precursors. Environ. Sci. Technol. 52, 2810–2818.

Li, K., Jacob, D.J., Liao, H., Shen, L., Bates, K.H., 2019. Anthropogenic drivers of 2013–2017 trends in summer surface ozone in China. Proc. Natl. Acad. Sci. 116 (2), 422–427.

Lin, Y., Jiang, F., Zhao, J., Zhu, G., He, X., Ma, X., et al., 2018. Impacts of O3 on premature mortality and crop yield loss across China. Atmos. Environ. 194, 41–47.

Ling, Z.H., Guo, H., Zheng, J.Y., Louie, P.K.K., Cheng, H.R., Jiang, F., et al., 2013. Establishing a conceptual model for photochemical ozone pollution in subtropical Hong Kong. Atmos. Environ. 76, 208–220.

Lu, K., Zhang, Y., Su, H., Shao, M., Zeng, L., Zhong, L., et al., 2010. Regional ozone pollution and key controlling factors of photochemical ozone production in Pearl River Delta during summer time. SCIENCE CHINA Chem. 53, 651–663.

Ma, Z., Xu, J., Quan, W., Zhang, Z., Lin, W., Xu, X., 2016. Significant increase of surface ozone at a rural site, north of eastern China. Atmos. Chem. Phys. 16, 3969–3977. https://doi.org/10.5194/acp-16-3969-2016.

Martin, R.V., Fiore, A.M., Van Donkelaar, A., 2004. Space-based diagnosis of surface ozone sensitivity to anthropogenic emissions. Geophys. Res. Lett. 31.

Ou, J., Yuan, Z., Zheng, J., Huang, Z., Shao, M., Li, Z., et al., 2016. Ambient ozone control in a photochemically active region: short-term despiking or long-term attainment? Environ. Sci. Technol. 50, 5720–5728.

Ran, L., Zhao, C., Xu, W., Han, M., Lu, X., Han, S., et al., 2012. Ozone production in summer in theme gacities of Tianjin and Shanghai, China: a comparative study. Atmos. Chem. Phys. 12, 7531–7542.

Richter, A., Burrows, J.P., Nüß, H., et al., 2005. Increase in tropospheric nitrogen dioxide over China observed from space[J]. Nature 437 (7055), 129.

Shao, M., Lu, S.H., Liu, Y., Xie, X., Chang, C.C., Huang, S., et al., 2009a. Volatile organic compounds measured in summer in Beijing and their role in ground-level ozone formation. J. Geophys. Res.-Atmos. 114.

Shao, M., Zhang, Y., Zeng, L., Tang, X., Zhang, J., Zhong, L., et al., 2009b. Ground-level ozone in the Pearl River Delta and the roles of VOC and NO(x) in its production. J. Environ. Manag. 90, 512–518.

Shindell, D.T., 2004. Southern hemisphere climate response to ozone changes and greenhouse gas increases. Geophys. Res. Lett. 31.

Sillman, S., 2002. Some theoretical results concerning O3-NOx-VOC chemistry and NOx-VOC indicators. J. Geophys. Res. 107.

Sillman, S., 2003. O3-NOx-VOC sensitivity and NOx-VOC indicators in Paris: results from models and atmospheric pollution over the Paris area (ESQUIF) measurements. J. Geophys. Res. 108.

Sillman, S., West, J.J., 2009. Reactive nitrogen in Mexico City and its relation to ozone-precursor sensitivity: results from photochemical models. Atmos. Chem. Phys. 9, 3477–3489.

Song, C., Wu, L., Xie, Y., He, J., Chen, X., Wang, T., et al., 2017. Air pollution in China: status and spatiotemporal variations. Environ. Pollut. 227, 334–347.

Sun, Y., Wang, L., Wang, Y., Quan, L., Zirui, L., 2011. In situ measurements of SO2, NOx, NOy, and O3 in Beijing, China during August 2008. Sci. Total Environ. 409, 933–940.

Sun, L., Xue, L., Wang, T., Gao, J., Ding, A., Cooper, O.R., Lin, M., Xu, P., Wang, Z., Wang, X., Wen, L., Zhu, Y., Chen, T., Yang, L., Wang, Y., Chen, J., Wang, W., 2016. Significant

increase of summertime ozone at mount tai in central eastern China. Atmos. Chem. Phys. 16, 10637–10650. https://doi.org/10.5194/acp-16-10637-2016.
Sun, L., Xue, L., Wang, Y., Li, L., Lin, J., Ni, R., Yan, Y., Chen, L., Li, J., Zhang, Q., Wang, W., 2019. Impacts of meteorology and emissions on summertime surface ozone increases over central eastern China between 2003 and 2015. Atmos. Chem. Phys. 19, 1455–1469. https://doi.org/10.5194/acp-19-1455-2019.
Tang, G., Wang, Y., Li, X., Ji, D., Hsu, S., Gao, X., 2012. Spatial-temporal variations in surface ozone in northern China as observed during 2009-2010 and possible implications for future air quality control strategies. Atmos. Chem. Phys. 12, 2757–2776. https://doi.org/10.5194/acp-12-2757-2012.
Tie, X., Geng, F., Peng, L., Gao, W., Zhao, C., 2009. Measurement and modeling of O3 variability in Shanghai, China: application of theWRF-Chem model. Atmos. Environ. 43, 4289–4302.
Wang, S., Hao, J., 2012. Air quality management in China: issues, challenges, and options. J. Environ. Sci. 24, 2–13.
Wang, X.S., Li, J.L., Zhang, Y.H., Xie, S.D., Tang, X.Y., 2009. Ozone source attribution during a severe photochemical smog episode in Beijing, China. Sci. China, Ser. B: Chem. 52, 1270–1280.
Wang, T., Nie, W., Gao, J., Xue, L.K., Gao, X.M., Wang, X.F., et al., 2010. Air quality during the 2008 Beijing Olympics: secondary pollutants and regional impact. Atmos. Chem. Phys. 10, 7603–7615.
Wang, N., Guo, H., Jiang, F., Ling, Z.H., Wang, T., 2015. Simulation of ozone formation at different elevations in mountainous area of Hong Kong using WRF-CMAQ model. Sci. Total Environ. 505, 939–951.
Wang, N., Lyu, X.P., Deng, X.J., Guo, H., Deng, T., Li, Y., et al., 2016. Assessment of regional air quality resulting from emission control in the Pearl River Delta region, southern China. Sci. Total Environ. 573, 1554–1565.
Wang, T., Xue, L., Brimblecombe, P., Lam, Y.F., Li, L., Zhang, L., 2017. Ozone pollution in China: a review of concentrations, meteorological influences, chemical precursors, and effects. Sci. Total Environ. 575, 1582–1596.
Wang, N., Ling, Z.H., Deng, X.J., Deng, T., Lyu, X.P., Li, T.Y., et al., 2018a. Source contributions to PM2.5 under unfavorable weather conditions in Guangzhou City, China. Adv. Atmos. Sci. 35, 1145–1159.
Wang, Y., Guo, H., Zou, S., Lyu, X., Ling, Z., Cheng, H., et al., 2018b. Surface O3 photochemistry over the South China Sea: application of a near-explicit chemical mechanism box model. Environ. Pollut. 234, 155–166.
Watson, R.T., Rodhe, H., Oeschger, H., Siegenthaler, U., 1990. Greenhouse gases and aerosols. Climate change: the IPCC scientific assessment. 1, p. 17.
Xie, M., Zhu, K., Wang, T., Yang, H., Zhuang, B., Li, S., et al., 2014. Application of photochemical indicators to evaluate ozone nonlinear chemistry and pollution control countermeasure in China. Atmos. Environ. 99, 466–473.
Xing, J., Wang, S.X., Jang, C., Zhu, Y., Hao, J.M., 2011. Nonlinear response of ozone to precursor emission changes in China: a modeling study using response surface methodology. Atmos. Chem. Phys. 11 (10), 5027–5044. https://doi.org/10.5194/acp-11-5027-2011.
Xu, Z.N., Huang, X., Nie, W., Chi, X.G., Xu, Z., Zheng, L.F., et al., 2017. Influence of synoptic condition and holiday effects on VOCs and ozone production in the Yangtze River Delta region, China. Atmos. Environ. 168, 112–124.
Xue, L.K., Wang, T., Gao, J., Ding, A.J., Zhou, X.H., Blake, D.R., et al., 2014. Ground-level ozone in four Chinese cities: precursors, regional transport and heterogeneous processes. Atmos. Chem. Phys. 14, 13175–13188.
Zhang, Q., Streets, D.G., Carmichael, G.R., He, K.B., Huo, H., Kannari, A., Klimont, Z., Park, I.S., Reddy, S., Fu, J.S., Chen, D., Duan, L., Lei, Y., Wang, L.T., Yao, Z.L., 2009. Asian emissions in 2006 for the NASA INTEX-B mission. Atmos. Chem. Phys. 9, 5131–5153.
Zhao, B., Wang, S., Dong, X., Wang, J., Duan, L., Fu, X., et al., 2013a. Environmental effects of the recent emission changes in China: implications for particulate matter pollution and soil acidification. Environ. Res. Lett. 8 (0), 24031.
Zhao, B., Wang, S.X., Liu, H., Xu, J.Y., Fu, K., Klimont, Z., et al., 2013b. NO_x emissions in China: historical trends and future perspectives. Atmos. Chem. Phys. 13, 9869–9897.
Zheng, B., Tong, D., Li, M., Liu, F., Hong, C., Geng, G., et al., 2018. Trends in China's anthropogenic emissions since 2010 as the consequence of clean air actions. Atmos. Chem. Phys. 18, 14095–14111.
Zhong, L.J., Louie, P.K.K., Zheng, J.Y., Yuan, Z.B., Yue, D.L., Ho, J.W.K., et al., 2013. Science-policy interplay: air quality management in the Pearl River Delta region and Hong Kong. Atmos. Environ. 76, 3–10.